Available online at www.sciencedirect.com
SCIENCE DIRECT®
Carbohydrate Research 339 (2004) 1331–1338
Carbohydrate RESEARCH

A conformational study of α-D-Man*p*-(1 → 2)-α-D-Man*p*-(1 → *O*)-L-Ser by NMR ^{1}H,^{1}H T-ROESY experiments and molecular-dynamics simulations

Kristina Lycknert,[a] Anne Helander,[b] Stefan Oscarson,[a] Lennart Kenne[c] and Göran Widmalm[a,*]

[a]*Department of Organic Chemistry, Arrhenius Laboratory, Stockholm University, S-106 91 Stockholm, Sweden*
[b]*Q-Med AB, Seminariegatan 21, S-752 28 Uppsala, Sweden*
[c]*Department of Chemistry, Swedish University of Agricultural Sciences, Box 7015, S-750 07 Uppsala, Sweden*

Received 12 January 2004; received in revised form 20 February 2004; accepted 28 February 2004

Available online 25 March 2004

Abstract—The conformational preference of α-D-Man*p*-(1 → 2)-α-D-Man*p*-(1 → *O*)-L-Ser has been investigated by one-dimensional ^{1}H,^{1}H T-ROESY experiments and molecular-dynamics simulations with CHARMM22 type of force fields and water as explicit solvent. Proton–proton distances were obtained from the simulations and subsequently experimentally determined distances could be derived. Measurements were performed on the title compound as well as on selectively deuterium-substituted analogues synthesized as part of this study to alleviate possible NMR spectroscopic difficulties. A very good agreement was present between the separate NMR experiments. In the subsequent analysis a key nuclear Overhauser effect between the anomeric protons in the two sugar residues was used to assess the conformational dynamics revealed by the molecular simulations. The combined results support a model in which two states are significantly populated as a result of flexibility around the bond defined by the glycosidic torsion angle ψ.

Keywords: Dynamics; Flexibility; Glycosylation; *Saccharomyces cerevisiae*

1. Introduction

Glycosylation of proteins plays an important part in protein folding,[1] trafficking,[2] and stability.[3] Several ways of conjugation to an amino acid side chain are known where the most commonly observed are those to an asparagine residue[4] or to serine or threonine.[5] Even C-glycosylation of a mannosyl residue to tryptophan in an intact protein has been described.[6]

O-Glycosylation is often present via an *N*-acetylgalactosamine residue, for example, in the T-antigen or in the GlyCAM-1 glycoprotein.[7] However, other sugar residues, such as mannose, have been found to be O-linked, for example, in brain tissue[8] and in glycoproteins from yeast and mould.[9] Some time ago it was shown that the human insulin-like growth factor I expressed in *Saccharomyces cerevisiae* contained a glycosylated variant with α-D-Man*p*-(1 → 2)-α-D-Man*p*-(1 → linked to L-threonine.[10]

Subsequently, conformational studies of the synthetically prepared above disaccharide linked to L-threonine and L-serine were performed by NMR ^{1}H,^{1}H steady-state NOE experiments as well as chemical shift analysis in conjunction with Metropolis Monte Carlo simulations employing the HSEA approach.[11] It was demonstrated that the fit between experimental and simulated NOE data was improved when ensemble averaging from the MMC simulations was taken into account.

* Corresponding author. Tel.: +46-8-16-37-42; fax: +46-8-15-49-08; e-mail: gw@organ.su.se

0008-6215/$ - see front matter © 2004 Elsevier Ltd. All rights reserved.
doi:10.1016/j.carres.2004.02.022

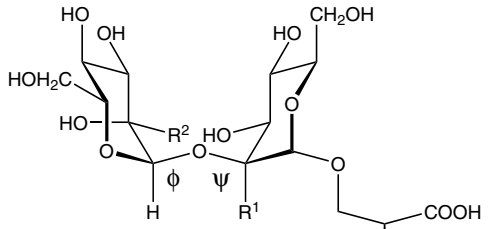

1 R^1 = H, R^2 = H
1-*d* R^1 = D, R^2 = H
1-*d*$_2$ R^1 = D, R^2 = D

Figure 1. Schematic of disaccharides with glycosidic torsion angles denoted as ϕ and ψ.

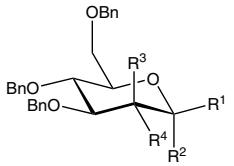

2 R^1 = SEt, R^2 = H, R^3 = H, R^4 = OH
3-*d* R^1 = SEt, R^2 = H, R^3 = OH, R^4 = D
4-*d* R^1 = SEt, R^2 = H, R^3 = OBn, R^4 = D
5 R^1 = H, R^2 = Br, R^3 = OBn, R^4 = H
5-*d* R^1 = H, R^2 = Br, R^3 = OBn, R^4 = D

Figure 2. Key monosaccharide derivatives used in the synthesis of deuterated disaccharides.

In the present study we extend the previous investigation by analysis of α-D-Man*p*-(1 → 2)-α-D-Man*p*-(1 → *O*)-L-Ser **1** and its deuterated analogues **1**-*d* and **1**-d_2 (Fig. 1). The current approach is similar to that in the previous study, except that we use one-dimensional ^{1}H,^{1}H T-ROESY experiments and molecular-dynamics simulations with explicit water as solvent. In particular, we analyze the conformational flexibility at the α-(1 → 2)-linkage.

2. Results and discussion

In a conformational analysis of a similar system to **1**, namely α-L-Rha*p*-(1 → 2)-α-L-Rha*p*-OMe, it was found that the H-1′–H-1 NOE could be useful for distinguishing a conformational preference, in particular, at the ψ torsion angle.[12] Furthermore, it was shown that under certain experimental conditions some conformations could lead to significant 'three-spin effects', which may be incorrectly interpreted in the form of a conformational preference. However, if the intervening proton is replaced by a deuterium, the possible relayed relaxation can be ignored. In the present extended study of α-D-Man*p*-(1 → 2)-α-D-Man*p*-(1 → O)-L-Ser we therefore synthesize deuterium-substituted analogues.

Deuterium substitution was performed by reduction with $NaCNBD_3$ of ethyl 3,4,6-tri-*O*-benzyl-thio-β-D-*arabino*-hexopyranosid-2-ulose obtained by oxidation with oxalyl chloride/DMSO of ethyl 3,4,6-tri-*O*-benzyl-1-thio-β-D-glucopyranoside **2** to give ethyl 3,4,6-tri-*O*-benzyl-1-thio-β-D-(2-^{2}H)-mannopyranoside **3**-*d* (Fig. 2). Treatment of the latter compound with sodium hydride and benzyl bromide gave ethyl 2,3,4,6-tetra-*O*-benzyl-1-thio-β-D-(2-^{2}H)-mannopyranoside **4**-*d*. The glycosyl acceptor **3**-*d* was used in a silver triflate-promoted coupling with the bromide **5**-*d* as well as with its nondeuterated analogue **5**. Subsequent methyl triflate-assisted couplings to a protected L-serine derivative gave after deprotection **1**-*d* and **1**-d_2, respectively.

One-dimensional ^{1}H,^{1}H T-ROESY spectra were used to obtain cross-relaxation build-up curves generated from experiments with different mixing times (Fig. 3). The cross-relaxation rates, σ, were obtained by fitting to a second-order polynomial. When the dynamics of the molecule is unknown but an appropriate reference distance (r_{ref}) can be obtained from, for example, molecular simulations the unknown distance (r_{ij}) in the molecule can be found by application of the isolated spin-pair approximation (ISPA)[13] according to: $r_{ij} = r_{ref}(\sigma_{ref}/\sigma_{ij})^{1/6}$. The resulting *trans*-glycosidic proton distances are given in Table 1, where the H-1′–H-2′ distance of 2.53 Å, obtained from MD simulations (vide infra), in **1** was used as reference. For distances <2.7 Å the agreement between the three substances is excellent when a comparison is possible and very good for distances >2.7 Å. In particular, the H-1′–H-1 distance is 3.13 ± 0.07 Å. The shorter distances across the glycosidic linkage show an H-1′–H-2 distance of 2.25 Å and the H-1–H-5′ distance as 2.60 ± 0.01 Å. Correlations are also observed for H-1 to the β-protons of the L-serine residue with average values of 2.84 and 2.37 Å (Table 1). Employing the MD simulations discussed below it was

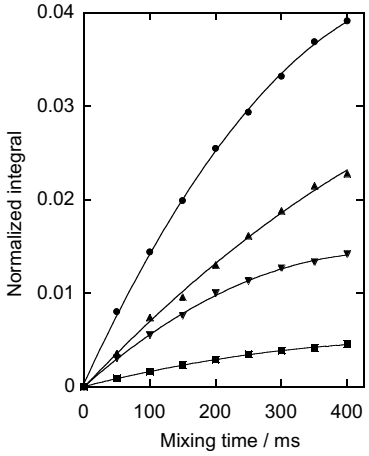

Figure 3. ^{1}H,^{1}H cross-relaxation build-up curves obtained from the 1D ^{1}H,^{1}H T-ROESY spectra: H-1′–H-2 in **1** (●), H-1′–H-2′ in **1** (▲), H-1–H-5′ in **1**-*d* (▼), and H-1–H-1′ in **1**-*d* (■). The first proton of each pair was selectively excited. The subsequently derived cross-relaxation rates σ (s^{-1}) were: 0.152 (●), 0.074 (▲), 0.062 (▼), and 0.018 (■).

Table 1. Proton–proton distances r (Å) for the disaccharides derived from 1D ^{1}H,^{1}H T-ROESY NMR experiments using ISPA and from the MD simulations using the PARM22 (I and II) and PARM22/SU01 (III and IV) force fields[a]

Proton pair	**1**	**1**-*d*	**1**-d_2	I	II	III	IV
H-1′–H-2	2.25	n.m.[b]	n.m.	2.39	2.37	2.36	2.32
H-1–H-5′	2.59	2.61	2.60	3.33	3.21	2.99	2.99
H-1–H-1′	3.06	3.19	3.14	2.48	2.54	2.74	2.76
H-1–H-$\beta_{pro\text{-}R}$	2.72	2.90	2.90	2.93	2.93	2.80	2.83
H-1–H-$\beta_{pro\text{-}S}$	2.36	2.37	2.38	2.41	2.43	2.41	2.40
H-1–H-2	2.54	n.m.	n.m.	2.50	2.51	2.50	2.51
H-1′–H-2′	2.53[c]	2.52	n.m.	2.51	2.51	2.53	2.53

[a] $r = \langle r^{-3} \rangle^{-1/3}$ from simulation.
[b] n.m.=not measurable.
[c] Reference distance from MD simulation.

possible to assign the resonances of the β-protons at δ_H 4.12 and 3.88 to H-$\beta_{pro\text{-}R}$ and H-$\beta_{pro\text{-}S}$, respectively.

Molecular-dynamics (MD) simulations of **1** were carried out with explicit water starting with different initial conditions. The first simulation was carried out for 3 ns. The average glycosidic torsion angles were $\langle \phi \rangle = -33°$ and $\langle \psi \rangle = 62°$, with the probability distribution as shown in Figure 4. The disaccharide may from these results be described as existing in a single dynamic conformation.[14] In the earlier MMC simulations using the HSEA approach $\langle \psi \rangle \approx 0°$, that is, a quite substantial difference to the simulation results obtained from MD. The H-1′–H-1 distance is the parameter most sensitive to conformational changes at the ψ torsion angle, as seen in Figure 5. The experimentally determined distance (3.13 Å) suggests a conformational preference for a region between those determined by MD simulation I and by MMC, if a conformation of limited flexibility is present. A second simulation, also employing the PARM22 force field resulted in highly similar averages for the glycosidic torsion angles (Table 2) as well as for the distances between different proton pairs (Table 1). Thus, the description of this single dynamic conformation may be regarded as well converged on the short nanosecond time scale.

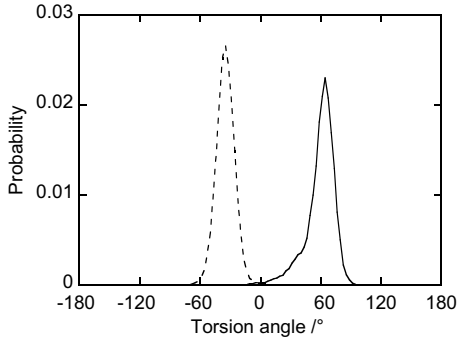

Figure 4. Probability distribution of the glycosidic torsion angles ϕ (- - -) and ψ (—) for **1** determined from MD simulation I with the PARM22 force field.

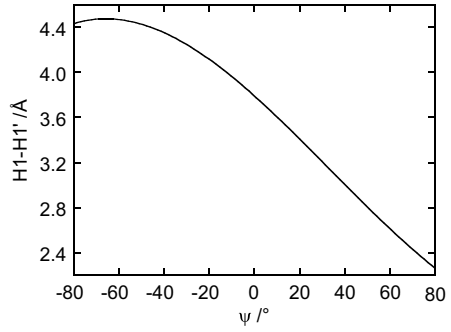

Figure 5. H-1–H-1′ distance dependence for **1** upon rotation of the glycosidic torsion angle ψ, taken at $\phi = -33°$ (cf. simulation I).

Table 2. Glycosidic torsion angle (°) averages of **1** from the MD simulations

Simulation	$\langle \phi \rangle$	$\langle \psi \rangle$
I	−33 (9)[a]	62 (15)
II	−34 (10)	59 (16)
III	−34 (16)	38 (35)
IV	−34 (12)	41 (29)

[a] Root-mean-square deviations in parentheses.

However, a conformational equilibrium between two or even more significantly populated states is also possible. MD simulations of α-D-Man*p*-(1→2)-α-D-Man*p*-(1→ as its *O*-methyl glycoside[15] and as a terminal disaccharide in a high-mannose type oligosaccharide ($Man_9GlcNAc_2$) indicated that it existed in a two-state conformational equilibrium where transitions occurred on a sub-nanosecond time scale.[16,17] Also, a similar two-state equilibrium has been reported for the α-(1→3)-linkage in an all mannose trisaccharide.[18]

We have recently performed an improvement of the PARM22 force field for carbohydrate applications.[19] In particular we addressed discrepancies evident from NMR data for glycosidic linkages with an equatorial group, that is, sugars like β-D-Glc*p*. During the development we also addressed linkages with an axial group, that is, sugars like α-D-Glc*p*, as well as the relative

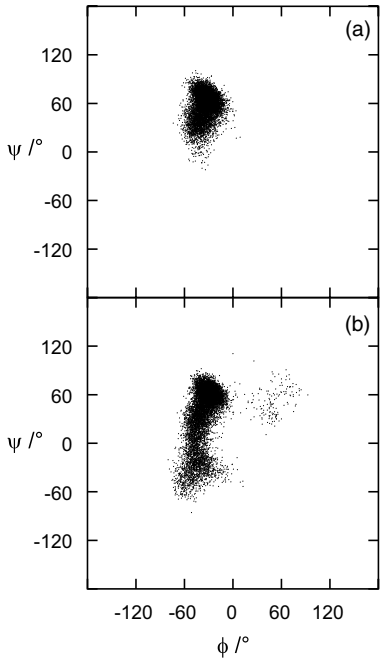

Figure 6. Scatter plots of ϕ versus ψ for **1** from MD simulations II (a) and III (b) using the PARM22 and PARM22/SU01 force fields, respectively.

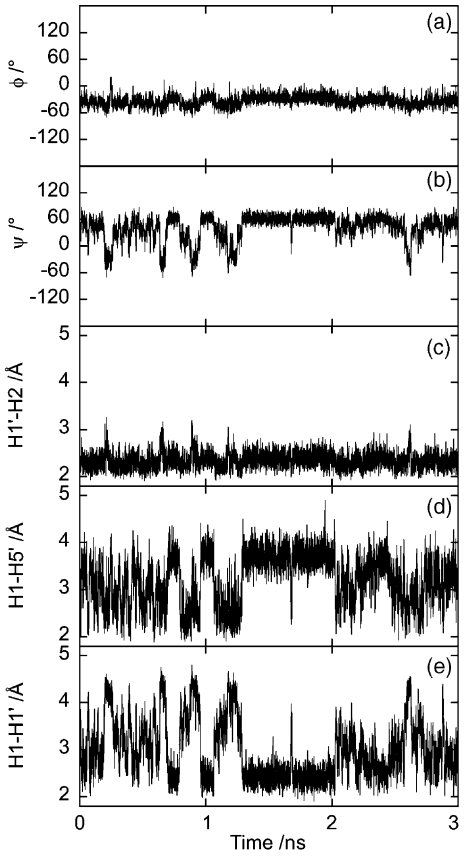

Figure 7. The time dependence for **1** showing the glycosidic torsion angles (a,b) as well as selected proton–proton distances (c–e) from simulation IV using the PARM22/SU01 force field.

populations of hydroxymethyl groups in some sugars. Herein, we test the new force field referred to as PARM22/SU01. Two MD simulations of similar duration as those described above were performed. The difference between the force fields is depicted by scatter plots in Figure 6. Whereas application of the PARM22 force field (simulations I and II) results in a single dynamic conformation, the PARM22/SU01 force field (simulations III and IV) leads to a larger flexibility that is obtained primarily at the ψ torsion angle (Fig. 6, but also to a limited extent at the ϕ torsion angle (non-*exo*-anomeric conformation).[20,21] The population of this conformational state may be addressed by analysis of the H-2′–H-2 interaction.[22] However, due to similar chemical shifts of the two protons this was not investigated in the present study. It is particularly evident from the time dependence of ψ in simulation IV (Fig. 7) that a two-state equilibrium is a suitable description for the conformational flexibility of the system. As a consequence of the conformational state in which the ψ torsion angle has a negative value, the average value of ψ is shifted $\sim$20° in the latter force field (Table 2). The glycosidic linkage at α-D-Man*p*-(1 → *O*)-L-Ser in simulation IV had $\langle\phi\rangle = -49°$, in agreement with an *exo*-anomeric conformation, and the C-1–O–C-β–C-α torsion angle in an anti-periplanar conformation, that is, close to 180° during the whole simulation. Recently, a computational study was presented using molecular-mechanics and ab initio methods on O-glycosides of serine derivatives in which both anti and eclipsed conformers were identified as the most stable rotamers.[23]

Comparison of the experimentally derived proton–proton distances and those calculated from the simulations can be used to (i) evaluate the force fields used and (ii) obtain an estimate of the population between different states (if present). For the two simulations of each force field the glycosidic torsion angles were similar and so were the calculated inter-proton distances (Table 1). The *trans*-glycosidic distance H-1′–H-2 is insensitive in the comparison (Fig. 7c). The H-1–H-5′ distance is overestimated in both force fields. On the other hand, the H-1–H-1′ distance is underestimated. These distances are anti-correlated (Fig. 7d and e) and dependent on the ψ torsion angle (Fig. 7b). However, the results obtained with the PARM22/SU01 force field are closer to the experimental data for both distances. Thus, a model in which the conformational equilibrium at ψ is present, is supported by the closer resemblance to experimental data. It must be kept in mind that since the number of transitions is limited during the 3 ns simulation the comparison cannot be extended too far. In order to obtain a statistically relevant evaluation for this system a longer simulation of at least an order of magnitude is necessary. Employing a two-state model one can estimate that an increase, compared to the present

simulation, of the conformational state with a negative ψ torsion angle is consistent with experimental data.

Hydrogen bonding in saccharides is an integral part in determining their conformation. However, they are often transient[24] and the predominant interaction is that of the solute and solvent molecules, usually water.[25] It was previously shown that some inter-residue hydrogen bonds were present in α-D-Man*p*-(1→2)-α-D-Man*p*-OMe.[15] Using geometric criteria we analyzed for possible hydrogen bonds in **1**. Initially, the dynamics of the hydroxymethyl groups were monitored, which revealed that all three conformational states were sampled, but that the major conformations were *gt* and *gg*, as anticipated (Fig. 8a and b). In order for a hydrogen bond to be present, the distance between the donor and the acceptor atoms should be short (<3.4 Å), which is the case between ~1.3 and 2.0 ns (Fig. 8c). The O-6–HO-6···O-6′ hydrogen bond was present 30% of the time in simulation IV. The O-6–HO-6···O-5′ and O-6′–HO-6′···O-6 hydrogen bonds were only present 3% and 1%, respectively. However, when ω has the *gg* conformation and ω′ the *gt* conformation, the geometric criteria are all fulfilled for the O-6–HO-6···O-6′ hydrogen bond (Fig. 8c–e), which is present to 92% during this part of the simulation. Thus, this conformational state with $\langle\psi\rangle = 62°$ and limited flexibility (rmsd=8°) leads to a well-defined state with a rigid conformation triggered and maintained by a strong hydrogen bond. Experimentally this interaction could be detected by NMR analysis of hydroxyl proton exchange at low temperatures.[26] However, although the hydrogen bond may be strong it would probably only be detected as a relatively weak interaction since the above ^{1}H,^{1}H T-ROESY data show that this conformation is not the single one.

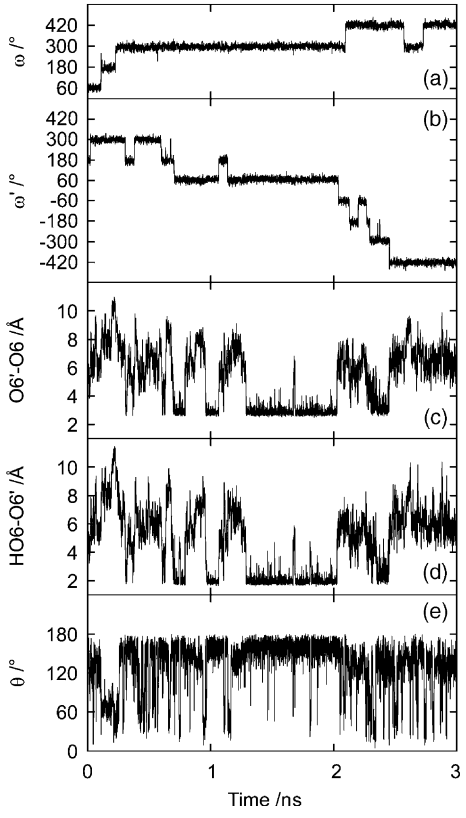

Figure 8. The time dependence from simulation IV of **1** showing the hydroxymethyl torsion angles (a,b), distances for atoms that may be involved in inter-residue hydrogen bonding (c,d), and the angle O-6–HO-6–O-6′ (e).

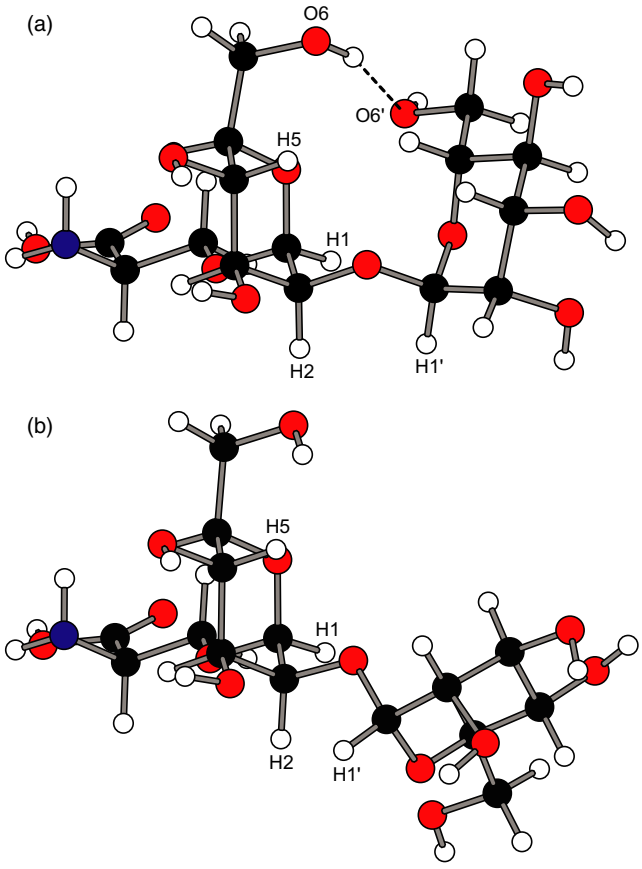

Figure 9. Molecular model of **1** indicating the flexibility at the glycosidic torsion angle ψ, as a result of two significantly populated conformational states: (a) $\langle\psi^+\rangle = 49°$ and (b) $\langle\psi^-\rangle = -26°$ (simulation IV). Protons used in the characterization of the conformational dynamics at the α-(1→2)-linkage are annotated.

In conclusion, from NMR spectroscopy and molecular simulations it is evident that two major states are in dynamical equilibrium (Fig. 9). In addition, the non-*exo*-anomeric conformation was also sampled in one of the MD simulations. Furthermore, inter-residue hydrogen bonding may stabilize flexible parts into quite rigid conformations, a mechanism that may be of considerable importance in large oligosaccharides. The results presented herein further exemplify the duality of oligosaccharide dynamics, that is, that they can be viewed as both rigid and (highly) flexible depending on the time scale considered.[27]

3. Experimental

3.1. General

Synthesis of **1** was described previously together with chemical shift assignments of its ^{1}H and ^{13}C NMR resonances.[11] Atoms of the terminal mannosyl residue are designated with a prime and those in the *O*-methyl mannoside are unprimed. The torsion angles across the glycosidic linkage are defined for ϕ as H-1′–C-1′–O-2′–C-2 and for ψ as C-1′–O-2′–C-2–H-2. The torsion angle of the hydroxymethyl group ω is defined by the atoms O-5–C-5–C-6–O-6.

3.2. Synthesis

3.2.1. Ethyl 2,3,4,6-tetra-*O*-benzyl-1-thio-β-D-(2-^{2}H)-mannopyranoside 4-*d*. Ethyl 3,4,6-tri-*O*-benzyl-1-thio-β-D-glucopyranoside **2**[28] (494 mg, 1 mmol) was dissolved in CH_2Cl_2 (25 mL) and the solution cooled to −60 °C. A solution of oxalyl chloride (100 mL, 1.1 mmol) and DMSO (170 mL, 2.2 mmol) in CH_2Cl_2 (5 mL) was added dropwise and after 15 min Et_3N (0.7 mL, 5 mmol). The mixture was allowed to attain room temperature. The reaction mixture was washed with water and brine, dried ($NaHSO_4$), filtered, and concentrated. The residue was dissolved in MeOH (10 mL) and $NaCNBD_3$ (66 mg, 1 mmol) was added and the mixture stirred for 15 min, whereafter it was concentrated and the residue purified on a silica gel column (toluene/EtOAc, 8:1) to give ethyl 3,4,6-tri-*O*-benzyl-1-thio-β-D-(2-^{2}H)-mannopyranoside **3**-*d* (340 mg, 0.7 mmol, 69%) and also 30 mg (6%) of the corresponding *gluco*-isomer. Compound **3**-*d* was crystallized from diethyl ether/light petroleum (bp 40–60 °C). To a solution of **3**-*d* (1 g, 2 mmol) in DMF (15 mL) was added NaH (80%, 100 mg, 3 mmol) and then dropwise a solution of benzyl bromide (0.47 mL, 3 mmol) in DMF (3 mL). After 30 min, MeOH (5 mL) was added to the mixture, which was then concentrated and purified by silica gel chromatography (toluene/EtOAc, 30:1) to give **4**-*d* (1 g, 1.7 mmol, 84%). Compound **4**-*d* was crystallized from diethyl ether/light petroleum (bp 40–60 °C). ^{13}C NMR ($CDCl_3$): 15.4, 26.0, 69.9, 72.7, 73.4, 74.9, 75.2, 80.2, 84.3, 84.4, 127.5–138.5. ^{1}H NMR ($CDCl_3$): 1.30 (t), 2.73 (q), 3.52 (m, H-5), 3.62 (d, H-3), 3.71–3.87 (m, H-6a, H-6b), 3.96 (dd, H-4), 4.53–5.03 (4×CH_2, H-1), 7.20–7.55 (aromatic H). The consecutive glycosylations to the serine containing disaccharides were performed as described previously.[11]

3.3. NMR spectroscopy

The disaccharides were treated with CHELEX 100 in order to remove any paramagnetic ions. The samples were freeze dried and dissolved in 0.7 mL D_2O to give a total concentration of ~20 mM, transferred to 5 mm NMR tubes, and flame sealed under vacuum after degassing by three freeze–pump–thaw cycles. NMR experiments were performed on a Varian INOVA 600 spectrometer.

Proton–proton cross-relaxation rates (σ) were measured at 303 K using one-dimensional DPFGSE T-ROESY experiments.[29] Selective excitations were enabled using 25–15 Hz broad i-Snob-2 shaped pulses[30] of 68–113 ms duration. The gradient durations in the initial DPFGSE part were 1 ms and the strengths 0.8 and 2.3 G cm^{-1}, respectively. The DPFGSE part was followed by a T-ROESY spin lock with $\gamma B_1/2\pi = 2.5$ kHz. Spectra were recorded using a width of 1200 Hz and 4800 complex points. For each mixing time, 944 transients were used and the total relaxation delay between the transients was 10 s, which corresponds to $> 5T_1$. Ten different ^{1}H, ^{1}H cross-relaxation delays (mixing times) between 50 and 800 ms were used. Prior to Fourier transformation the FIDs were zero filled and multiplied with a 1 Hz exponential line-broadening factor. Spectra were phased, drift corrected and baseline corrected using a first-order correction, and integrated using the same integration limits at all mixing times.

Integrated auto-peaks were fitted to an exponentially decaying function. Normalized integrals of cross-relaxation peaks were obtained by division of the measured integrals by the extrapolated auto-peak value at zero mixing time. The regression coefficient in the fits was $R > 0.999$ for all auto-peaks. Cross-relaxation build-up curves were obtained from the normalized integrals at different mixing times and the rates were calculated by fitting to a second-order polynomial up to 400 ms. The least-square fits, expressed using the regression coefficient, showed $R > 0.982$ in all cases. When possible, each distance reported in Table 1 (vide infra) is an average of the two cross-relaxation rates obtained from excitations at the different proton resonance frequencies of a proton pair, for example, in **1** from H-1 to H-1′ and vice versa. Additional measurements on **1**-*d* and **1**-d_2 were used to estimate the precision in the derived distances.

3.4. Molecular simulations

MD simulations used CHARMM[31] (parallel version, C27b4) employing a CHARMM22 type of force field,[32] namely the PARM22 force field (Molecular Simulations Inc., San Diego, CA, USA), or a modification for carbohydrates referred to as PARM22/SU01.[19] Initial conditions were prepared by placing disaccharide **1** in a previously equilibrated cubic water box of length 29.97 Å containing 900 modified TIP3P water[33] molecules, and removing the solvent molecules that were closer than 2.5 Å to any solute atom. This procedure resulted in a system with the disaccharide and 871 water molecules. Energy minimization was performed with

Steepest Descent, 200 steps, followed by Adopted Basis Newton–Raphson until the root-mean-square gradient was less than 0.01 kcal mol^{-1} Å^{-1}. The MD simulations were carried out with the leap-frog algorithm[34] and a dielectric constant of unity. Initial velocities were assigned at 103 K, followed by heating at 5 K increments during 8 ps to 313 K, where the system was equilibrated for 200 ps. Four simulations were performed in which the production runs were temperature scaled by Berendsen's weak coupling algorithm,[35] namely, (I) a time step of 2 fs, the PARM22 force field and a duration of 3 ns; (II) a time step of 1 fs, the PARM22 force field and a duration of 1 ns; (III) a time step of 2 fs, the PARM22/SU01 force field and a duration of 2 ns; (IV) a time step of 1 fs, the PARM22/SU01 force field and a duration of 3 ns. Data were saved every 100 time steps for analysis. The simulations with the longer time step of 2 fs used SHAKE to restrain hydrogen heavy atom bonds[36] with a tolerance gradient of 10^{-4}. Periodic boundary conditions and the minimum image convention were used together with a heuristic nonbond frequency update and a force shift cutoff[37] acting to 12 Å. The geometric criteria for hydrogen bonding were set to an oxygen–hydrogen distance <2.5 Å and a donor-hydrogen$\cdots$acceptor angle $>135°$. Besides hydrogen bond analysis over the 3 ns of simulation IV, a limited analysis was carried out for the 1.3–1.6 and 1.7–2.0 ns segments. Simulations were performed on an IBM SP2 computer at the Center for Parallel Computers, KTH, Stockholm, using 16 nodes; this resulted in a CPU time of approximately 40 h/ns when a time step of 1 fs was employed.

Acknowledgements

This work was supported by grants from the Swedish Research Council (VR). We thank the Center for Parallel Computers, KTH, Stockholm, for putting computer facilities at our disposal.

References

1. Lige, B.; Ma, S.; van Huystee, R. B. *Arch. Biochem. Biophys.* **2001**, *386*, 17–24.
2. Opat, A. S.; Houghton, F.; Gleeson, P. A. *Biochem. J.* **2001**, *358*, 33–40.
3. Mer, G.; Hietter, H.; Lefèvre, J.-F. *Nat. Struct. Biol.* **1996**, *3*, 45–53, 298.
4. Gutiérrez Gallego, R.; Jiménez Blanco, J. L.; Thijssen-van Zuylen, C. W. E. M.; Gotfredsen, C. H.; Voshol, H.; Duus, J. Ø.; Schachner, M.; Vliegenthart, J. F. G. *J. Biol. Chem.* **2001**, *276*, 30834–30844.
5. Thomson, K. A.; Carlstedt, I.; Karlsson, N. G.; Karlsson, H.; Hansson, G. C. *Glycoconjugate J.* **1998**, *15*, 823–833.
6. Löffler, A.; Doucey, M.-A.; Jansson, A. M.; Müller, D. R.; de Beer, T.; Hess, D.; Meldal, M.; Richter, W. J.; Vliegenthart, J. F. G.; Hofsteenge, J. *Biochemistry* **1996**, *35*, 12005–12014.
7. Hemmerich, S.; Leffler, H.; Rosen, S. D. *J. Biol. Chem.* **1995**, *270*, 12035–12047.
8. Yuen, C.-T.; Chai, W.; Loveless, R. W.; Lawson, A. M.; Margolis, R. U.; Feizi, T. *J. Biol. Chem.* **1997**, *272*, 8924–8931.
9. Montreuil, J. *Adv. Carbohydr. Chem. Biochem.* **1980**, *37*, 157–233.
10. Gellerfors, P.; Axelsson, K.; Helander, A.; Johansson, S.; Kenne, L.; Lindqvist, S.; Pavlu, B.; Skottner, A.; Fryklund, L. *J. Biol. Chem.* **1989**, *264*, 11444–11449.
11. Helander, A.; Kenne, L.; Oscarson, S.; Peters, T.; Brisson, J.-R. *Carbohydr. Res.* **1992**, *230*, 299–318.
12. Widmalm, G.; Byrd, R. A.; Egan, W. *Carbohydr. Res.* **1992**, *229*, 195–211.
13. Keepers, J. W.; James, T. L. *J. Magn. Reson.* **1984**, *57*, 404–426.
14. Almond, A.; Duus, J. Ø. *J. Biomol. NMR* **2001**, *20*, 351–363.
15. Woods, R. J.; Edge, C. J.; Wormald, M. R.; Dwek, R. A. In *Complex Carbohydrates in Drug Research*; Bock, K., Clausen, H., Eds.; Munksgaard: Copenhagen, 1994; pp 15–26.
16. Woods, R. J.; Pathiaseril, A.; Wormald, M. R.; Edge, C. J.; Dwek, R. A. *Eur. J. Biochem.* **1998**, *258*, 372–386.
17. Wormald, M. R.; Petrescu, A. J.; Pao, Y.-L.; Glithero, A.; Elliott, T.; Dwek, R. A. *Chem. Rev.* **2002**, *102*, 371–386.
18. Sayers, E. W.; Prestegard, J. H. *Biophys. J.* **2000**, *79*, 3313–3329.
19. Eklund, R.; Widmalm, G. *Carbohydr. Res.* **2003**, *338*, 393–398.
20. Asensio, J. L.; Cañada, F. J.; Cheng, X.; Khan, N.; Mootoo, D. R.; Jiménez-Barbero, J. *Chem. Eur. J.* **2000**, *6*, 1035–1041.
21. Höög, C.; Widmalm, G. *J. Phys. Chem. A* **2000**, *104*, 9443–9447.
22. Espinosa, J.-F.; Bruix, M.; Jarreton, O.; Skrydstrup, T.; Beau, J.-M.; Jiménez-Barbero, J. *Chem. Eur. J.* **1999**, *5*, 442–448.
23. Csonka, G. I.; Schubert, G. A.; Perczel, A.; Sosa, C. P.; Csizmadia, I. G. *Chem. Eur. J.* **2002**, *8*, 4718–4733.
24. Vishnyakov, A.; Laaksonen, A.; Widmalm, G. *J. Mol. Graphics Modell.* **2001**, *19*, 338–342, 396–397.
25. Kirschner, K. N.; Woods, R. J. *Proc. Natl. Acad. Sci. U.S.A.* **2001**, *98*, 10541–10545.
26. Sandström, C.; Baumann, H.; Kenne, L. *J. Chem. Soc., Perkin Trans. 2* **1998**, 2385–2393.
27. Höög, C.; Landersjö, C.; Widmalm, G. *Chem. Eur. J.* **2001**, *7*, 3069–3077.
28. Ekelöf, K.; Oscarson, S. *J. Org. Chem.* **1996**, *61*, 7711–7718.
29. Kjellberg, A.; Widmalm, G. *Biopolymers* **1999**, *50*, 391–399.
30. Kupce, E.; Boyd, J.; Campbell, I. D. *J. Magn. Reson. B* **1995**, *106*, 300–303.
31. Brooks, B. R.; Bruccoleri, R. E.; Olafson, B. D.; States, D. J.; Swaminathan, S.; Karplus, M. *J. Comput. Chem.* **1983**, *4*, 187–217.
32. MacKerell, A. D., Jr.; Bashford, D.; Bellott, M.; Dunbrack, R. L., Jr.; Evanseck, J. D.; Field, M. J.; Fischer, S.; Gao, J.; Guo, H.; Ha, S.; Joseph-McCarthy, D.; Kushnir, L.; Kuczera, K.; Lau, F. T. K.; Mattos, C.; Michnick, S.; Ngo, T.; Nguyen, T. D.; Prodhom, B.; Reiher, W. E., III; Roux, B.; Schlenkrich, M.; Smith, J. C.; Stote, R.; Straub, J.; Watanabe, M.; Wiórkiewicz-Kuczera, J.; Yin, D.; Karplus, M. *J. Phys. Chem. B* **1998**, *102*, 3586–3616.
33. Neria, E.; Fischer, S.; Karplus, M. *J. Chem. Phys.* **1996**, *105*, 1902–1921.

34. Hockney, R. W. *Meth. Comput. Phys.* **1970**, *9*, 136–211.
35. Berendsen, H. J. C.; Postma, J. P. M.; van Gunsteren, W. F.; DiNola, A.; Haak, J. R. *J. Chem. Phys.* **1984**, *81*, 3684–3690.
36. Ryckaert, J. P.; Ciccotti, G.; Berendsen, H. J. C. *J. Comput. Phys.* **1977**, *23*, 327–341.
37. Steinbach, P. J.; Brooks, B. R. *J. Comput. Chem.* **1994**, *15*, 667–683.